3-9-2022

Oxygen Ion Escape at Venus Associated With Three-Dimensional Kelvin-Helmholtz Instability

Tong Dang
University of Science and Technology of China

Xuanye Ma
Embry-Riddle Aeronautical University, max@erau.edu

Jiuhou Le
University of Science and Technology of China

Binzheng Zhang
The University of Hong Kong

Tielong Zhang
Harbin Institute of Technology

See next page for additional authors

Scholarly Commons Citation

Dang, T., Lei, J., Zhang, B., Zhang, T., Yao, Z., Lyon, J., et al. (2022). Oxygen ion escape at Venus associated with three-dimensional Kelvin-Helmholtz instability. Geophysical Research Letters, 49, e2021GL096961. https://doi. org/10.1029/2021GL096961

AGU ADVANCING EARTH AND SPACE SCIENCE

Geophysical Research Letters®

RESEARCH LETTER
10.1029/2021GL096961

Key Points:

- We present the first three-dimensional (3D) Kelvin-Helmholtz instability (KHI) structures at the Venusian magnetospheric boundary layer with a high-resolution multifluid model
- The KHI is well resolved and exhibits dynamic and fine evolutions in the 3D global model
- KHI leads to significant escape of oxygen ions through mixing with the solar wind at the low latitude boundary layer of Venus

Supporting Information:

Supporting Information may be found in the online version of this article.

Correspondence to:

J. Lei,
leijh@ustc.edu.cn

Citation:

Dang, T., Lei, J., Zhang, B., Zhang, T., Yao, Z., Lyon, J., et al. (2022). Oxygen ion escape at Venus associated with three-dimensional Kelvin-Helmholtz instability. *Geophysical Research Letters*, *49*, e2021GL096961. https://doi.org/10.1029/2021GL096961

Received 8 NOV 2021
Accepted 6 MAR 2022

Oxygen Ion Escape at Venus Associated With Three-Dimensional Kelvin-Helmholtz Instability

Tong Dang[1,2,3], Jiuhou Lei[1,2,3], Binzheng Zhang[4], Tielong Zhang[5,6], Zhonghua Yao[7], John Lyon[8], Xuanye Ma[9], Sudong Xiao[5], Maodong Yan[1], Oliver Brambles[10], Kareem Sorathia[11], and Viacheslav Merkin[11]

[1]CAS Key Laboratory of Geospace Environment, School of Earth and Space Sciences, University of Science and Technology of China, Hefei, China, [2]CAS Center for Excellence in Comparative Planetology, Hefei, China, [3]Mengcheng National Geophysical Observatory, University of Science and Technology of China, Hefei, China, [4]Department of Earth Sciences, The University of Hong Kong, Hong Kong SAR, China, [5]Harbin Institute of Technology, Shenzhen, China, [6]Space Research Institute, Austrian Academy of Sciences, Graz, Austria, [7]Key Laboratory of Earth and Planetary Physics, Institute of Geology and Geophysics, Chinese Academy of Sciences, Beijing, China, [8]Department of Physics and Astronomy, Dartmouth College, Hanover, NH, USA, [9]Department of Physical Sciences and Center for Space and Atmospheric Research (CSAR), Embry-Riddle Aeronautical University, Daytona Beach, FL, USA, [10]O. J. Brambles Consulting, Preston, UK, [11]Applied Physics Laboratory, Johns Hopkins University, Laurel, MD, USA

Abstract How oxygens escape from Venus has long been a fundamental but controversial topic in the planetary research. Among various key mechanisms, the Kelvin-Helmholtz instability (KHI) has been suggested to play an important role in the oxygen ion escape from Venus. Limited by either scarce in-situ observations or simplified theoretical estimations, the mystery of oxygen ion escape process associated with KHI is still unsettled. Here we present the first three-dimensional configuration of KHI at Venus with a global multifluid magnetohydrodynamics model, showing a significantly fine structure and evolution of the KHI. KHI mainly occurred at the low latitude boundary layer if defining the interplanetary magnetic field-perpendicular plane as the equatorial plane, resulting in escaping oxygen ions through mixing with the solar wind at the Venusian boundary layer, with an escape rate around 4×10^{24} s^{-1}. The results provide new insights into the basic physical process of atmospheric loss at other unmagnetized planet.

Plain Language Summary Kelvin-Helmholtz instability (KHI) forms where there's a velocity difference across the interface between two fluids: For example, wind blowing over water. The KHI also commonly occurs when solar wind flows past a magnetized body. At Venus, the solar wind directly interacts with the Venusian ionosphere and KHI takes place at the induced magnetosphere. The KHI is often considered as an important source of ion escape and atmospheric loss of Venus, however, limited by either scarce satellite observations or simplified theoretical estimations, the mystery of the oxygen ion escape process associated with the KHI is still unsolved. In this letter, we present the first three-dimensional (3D) KHI structures at the Venusian boundary layer, with a newly-developed, global, high-resolution, magnetohydrodynamic model. The KHI is well resolved and exhibits fine evolutions in the 3D global model. We have also found that the KHI could lead to significant escape of oxygen ions through mixing with the solar wind at the low latitude boundary layer of Venus. The KHI-induced oxygen ion escape rate of 4×10^{24} s^{-1} is comparable to the previous observation estimations. The results illustrate new insights into the atmospheric loss at the unmagnetized planets.

1. Introduction

Venus, different from the Earth, is a hot and dry planet and lacks an intrinsic magnetic field. As the sister planet of the Earth, the long-term oxygen loss at Venus is always a fundamental theme of research, especially on account of the implication for the Earth's past, future and habitability (Lammer et al., 2008; Way et al., 2016). Different mechanisms have been identified to contribute to the oxygen escape process at Venus, such as thermal (Jeans) escape (Lammer et al., 2006), non-thermal photochemistry (Shizgal & Arkos, 1996), as well as the effects from the solar wind. The continually blowing solar wind interacts with Venusian upper atmosphere/ionosphere and removes oxygen via pickup process (Barabash et al., 2007; Luhmann et al., 2006, 2008) and Kelvin-Helmholtz instability (KHI) (Pope et al., 2009; Walker et al., 2011). The KHI is a fundamental process in planetary and

astrophysical plasma environment, formed by the velocity shear between different plasma medium. At Venus, KHI couples mass and energy from solar wind into the upper atmosphere and leads to ion escape through mixing with the solar wind at the Venusian boundary layer (e.g., Elphic & Ershkovich, 1984; Thomas & Winske, 1991; Wolff et al., 1980).

There has been considerable debate regarding the ion escape rate at Venus due to limited availability of in-situ satellite observations (Brace et al., 1987; Futaana et al., 2017; Knudsen & Miller, 1992; Lundin, 2011; Masunaga et al., 2011; Nordström et al., 2013). The estimated escape rates varied drastically from an order of 10^{23} s^{-1} to 10^{26} s^{-1}, depending on the data base, assumptions, analysis methods and energy range considered. Consequently, how the basic physical process such as KHI contributes to the escape rate of Venusian oxygen ions remains unclear. Although theoretical and two-dimensional numerical simulations have been conducted to investigate the KHI and the associated ion escape (Amerstorfer et al., 2007; Cloutier et al., 1983; Möstl et al., 2011; Li & Lu, 2019; Thomas & Winske, 1991; Terada et al., 2002), the limitation of two-dimension without a global configuration, however, restricts the exploration of where, how, and to what extent the oxygen ions escape with KHI at the Venusian boundary layer.

It is only through highly resolved three-dimensional (3D) boundary layer modeling of the Venus-solar wind interaction that we can unveil the property of KHI and the associated oxygen ion escape at Venus. Here we present the first 3D KHI structures at the Venusian boundary layer, using a global, high-resolution, multi-fluid magnetohydrodynamics (MHD) model for the interaction between the Venusian ionosphere and the upstream solar wind. The fine structure of KHI is well resolved in the 3D global model. We have addressed the pathway and the rate of the escaping oxygen ions from Venus through the KHI. The results are also of importance for other unmagnetized planets such as Mars which has more ongoing satellite observations.

2. Methods

2.1. Multifluid Venusian Ionosphere-Solar Wind Interaction Model

The Venus-solar wind interaction was performed using a multi-fluid, high-resolution global MHD model, based on the Grid Agnostic MHD for Extended Research Applications (GAMERA) code (Michael et al., 2021; Sorathia et al., 2020; Zhang et al., 2019). The model has high resolving power, enabled by sophisticated numerical algorithms (Zhang et al., 2019), which allowed us to not only resolve the fine structure of the KHI but also demonstrate its dynamic nature associated with the oxygen ion escape. The GAMERA code uses a seventh-order upwind reconstruction to compute the numerical fluxes at cell interfaces, together with the constraint transport method to maintain the divergence of the magnetic field down to round off. The multi-fluid equations allow each ion species to move under its own force balance in the parallel direction, while moving in the bulk **E×B** drift in the perpendicular direction through averaging the gyro-motions. The multifluid Venus model solves the continuity, momentum, and energy equations of four ion fluids (H^+, O^+, O_2^+, and CO_2^+) in addition to the magnetic induction equation:

$$\frac{\partial \rho_i}{\partial t} + \nabla \cdot (\rho_i \boldsymbol{u}_i) = S_i - L_i \tag{1}$$

$$\frac{\partial (\rho_i \boldsymbol{u}_i)}{\partial t} + \nabla \cdot (\rho_i \boldsymbol{u}_i \boldsymbol{u}_i + p_i \boldsymbol{I}) + \boldsymbol{F}_i^d = \rho_i \boldsymbol{G} - \rho_i \sum\nolimits_n \nu_{in} \boldsymbol{u}_i - L_i \boldsymbol{u}_i \tag{2}$$

$$\begin{aligned}\frac{\partial \varepsilon_i}{\partial t} + \nabla \cdot [\boldsymbol{u}_i (\varepsilon_i + p_i)] + \boldsymbol{u}_i \cdot \boldsymbol{F}_i^d = \rho_i \boldsymbol{u}_i \cdot \boldsymbol{G} + \rho_i \sum\nolimits_n \frac{\nu_{in} \boldsymbol{u}_i}{m_i + m_n} \left[3k (T_n - T_i) + m_n u_i^2\right] - \frac{1}{2} L_i u_i^2 \\ + \frac{k}{\gamma - 1} \left(\frac{S_i T_n - L_i T_i}{m_i} \right)\end{aligned} \tag{3}$$

$$\frac{\partial \boldsymbol{B}}{\partial t} = \nabla \times (\boldsymbol{u} \times \boldsymbol{B}) \tag{4}$$

where i and n denote the ion and neutral species, respectively. ρ_i $\boldsymbol{u}_i$, p_i, T_i, and ε_i are the mass density, velocity, pressure, temperature and energy of ion i; S_i and L_i are the ion production and loss rates; $\boldsymbol{F}_i^d$ is electromagnetic force. T_n is neutral temperature; $\boldsymbol{G}$ is vector of gravitational acceleration; k is Boltzmann constant; γ is the adiabatic index; m_i and m_n are the mean molecular mass of ion species i and neutral species n; ν_{in} is the collision

frequency between ion i and neutral n; $\boldsymbol{u}$ is the bulk velocity; $\boldsymbol{B}$ is the vector of magnetic field. The specification of S_i, L_i, ν_{in}, $\boldsymbol{F}_i^d$ and the chemical reactions are given in the Supporting Information. The magnetic resistivity, which is important in the collisional Venusian ionosphere at low altitude (Ma et al., 2013, 2020), is neglected in the magnetic induction equation, since we are concentrating on the boundary layer structures above 400 km under constant solar wind driving.

The neutral species considered in the model include O, CO_2, O_2, and H, which were adopted from Fox and Sung (2001). Thus, our results in this work represent the solar maximum condition. Figures S1 and S2 in Supporting Information S1 give the altitudinal profiles of photoionization rates, as well as the density and temperature of neutrals and ions along the subsolar line.

The model uses the Venus Solar Orbital (VSO) coordinate, in which the X axis is along the Venus-Sun line and the Z axis is perpendicular to the orbital plane. We use a computational grid of $256 \times 256 \times 256$ cells in the radial, polar, and azimuthal directions to perform high-resolution KHI simulation. The low-altitude boundary of the grid is set to be 100 km above the Venus surface. A spherical grid with a radius from 100 to 500 km above the Venus surface is applied as the Venusian ionosphere, with a radial resolution of 10 km. Above 500 km, the model has an ellipsoid-like grid, with a gradually increasing grid size in the radial direction. The grid resolution is around 10–30 km at the magnetopause boundary layer. The outer boundaries of X, Y, and Z axes are set to be between [−10, 4], [−6 6], and [−6 6] in the unit of Venus Radii (Rv), respectively. We assume a hard wall for ion velocity to ensure that no mass flux of plasma goes across the inner boundary, and zero gradient for magnetic field at the inner boundary. Moreover, we use a zero-gradient condition for the densities and temperatures for ions except H^+ at the outer boundary. An idealized upstream solar wind/interplanetary magnetic field (IMF) condition was used in this study: the solar wind density is 10 cm^{-3}, the IMF and the solar wind velocity are [0, 10, 0] nT and [−400, 0, 0] km/s in VSO coordinates, respectively.

2.2. Power Spectrum Analysis

The power spectrum analysis was widely used in the analysis of KHI wave properties in the terrestrial magnetosphere (Claudepierre et al., 2008; Merkin et al., 2013). In this work, we consider 10 min simulation data with an output time resolution of 0.01 min. The power spectral density was

$$P(f_j) = \frac{2dt}{N}|X_j|^2 \text{ for } j = 0, 1, \ldots, \frac{N}{2} \tag{5}$$

where

$$X_j = \sum_{k=0}^{N-1} x_k \exp\left(\frac{-2\pi j k}{N}\mathrm{i}\right) \text{ for } j = 0, 1, \ldots, N-1 \tag{6}$$

and

$$f_j = \frac{j}{N\,dt} \text{ for } j = 0, 1, \ldots, \frac{N}{2} \tag{7}$$

Here f_j are the discrete Fourier frequencies in Hz, dt is the sampling rate in seconds, N is the number of points in the time series x_k, and X_j is the discrete Fourier transform of the time series x_k. The power spectral density $P(f)$ is calculated as a function of frequency, at every spatial point in the simulation domain. Then, the integrated power (IP) over a given frequency band of interest $[f_a, f_b]$ at each spatial grid point can be derived by:

$$IP = \int_{f_a}^{f_b} P(f)\,df \tag{8}$$

Here if x_k is number density and has the unit of cm^{-3}, then the unit of $P(f_j)$ and IP are $cm^{-6}Hz^{-1}$ and cm^{-6}, respectively.

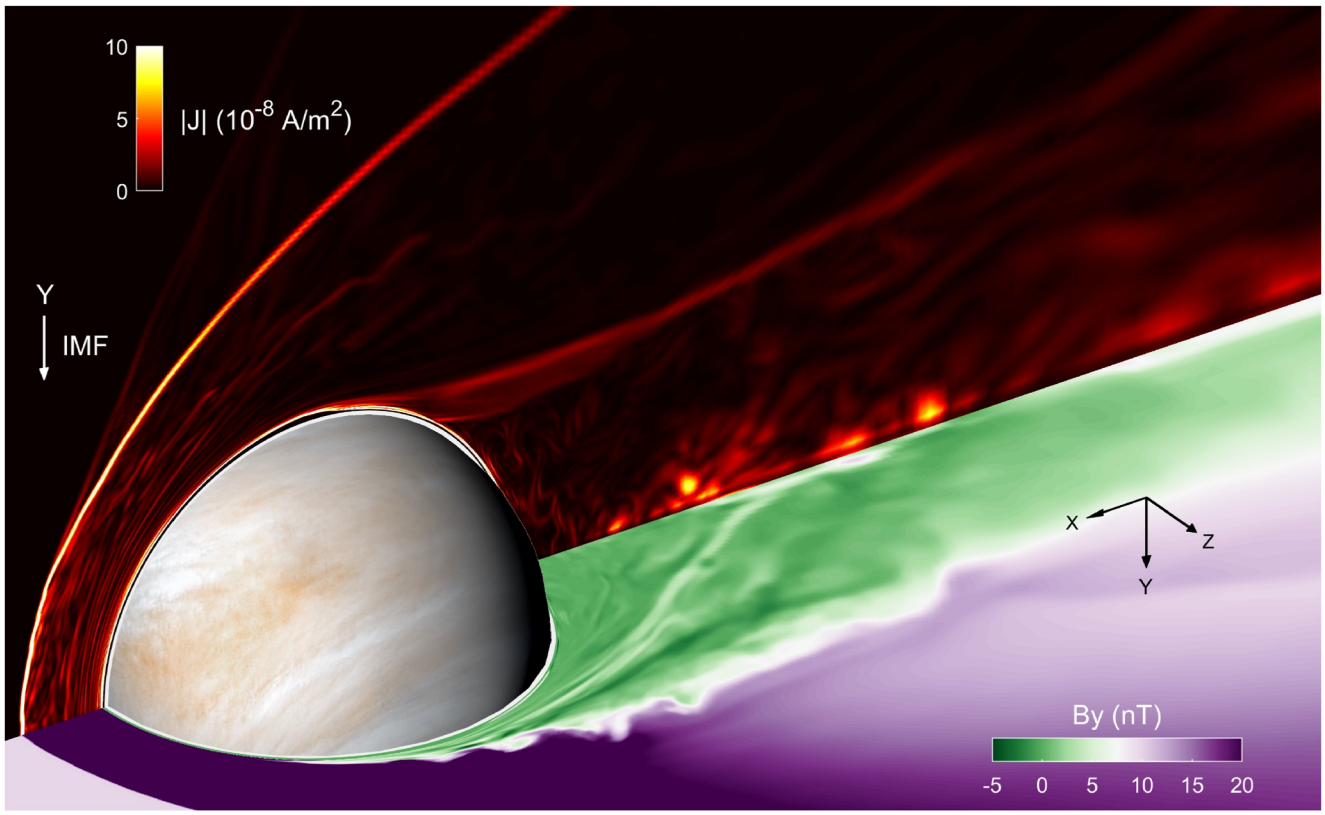

Figure 1. Overview of the three-dimensional Venusian space environment. The background shows the y component of the magnetic field in X-Z plane and electric current magnitude in X-Y plane at 13.8 min simulation time. The triad on the right of the figure indicates the axis orientation. See Movie S1 for the time evolution.

3. Results

Figure 1 displays a 3D snapshot of the surface waves at the boundary layer of Venus. The solar wind flows from the left with the IMF of (0,10,0) nT in the VSO coordinate, directly interacting with the Venusian ionosphere and forming an induced magnetosphere. Here the X-Z plane, which is perpendicular to the IMF, is the location of current sheet, and thus can be defined as the equatorial plane in comparison with the Earth. In the X-Z plane, surface waves occur near the flank region, associated with the KHI vortices. The wavelength of the perturbations along the boundary layer increases with distance down the tail. The dynamic evolution of the vortices from the dayside Venusian induced magnetosphere to the magnetotail is in Movie S1. Perturbations of the currents in the X-Y plane are evident with dynamic variations of current sheet. One can notice that there are O^+ density perturbations at high altitude in Figure S1 in Supporting Information S1. The wave signatures, seen in the electric current in Figure 1, are mainly associated with the compressional magnetosonic waves, which are continually excited by the shock and propagated into the upper ionosphere of Venus.

A snapshot of vortex structures near the Venusian boundary in the X-Z plane is shown in Figure 2. Here we use the number density of H^+, which is mainly from the solar wind, to show interactions between the solar wind and Venusian ionosphere and visualize the KHI. In Figures 2a and 2a density interface between solar wind/magnetosheath plasma and the induced magnetosphere is clearly identified, evolving with dynamic surface waves as seen in the Movie S2. Starting at around X = 0.4 Rv on the dayside, vortices are generated near the boundary layer. As advected further down tail, the vortices gradually decay. Those waves are associated with KHI and a detailed spectral analysis is performed in the following section. In the simulation, the radial cell size at the flank magnetopause is approximately 10 km, which allows us to resolve the boundary layer with about 10 cells across its width. This resolving power has demonstrated excellent effectiveness in Earth's KHI simulations along that magnetopause boundary (Merkin et al., 2013). The estimated width of the boundary layer (Figure 2a) ranges from around 800 km at the dayside to 2100 km at nightside tail. Besides KH surface waves, structures of low frequency standing wave are noted at X > 0.4 Rv in the magnetosheath. Variations of the y-component of

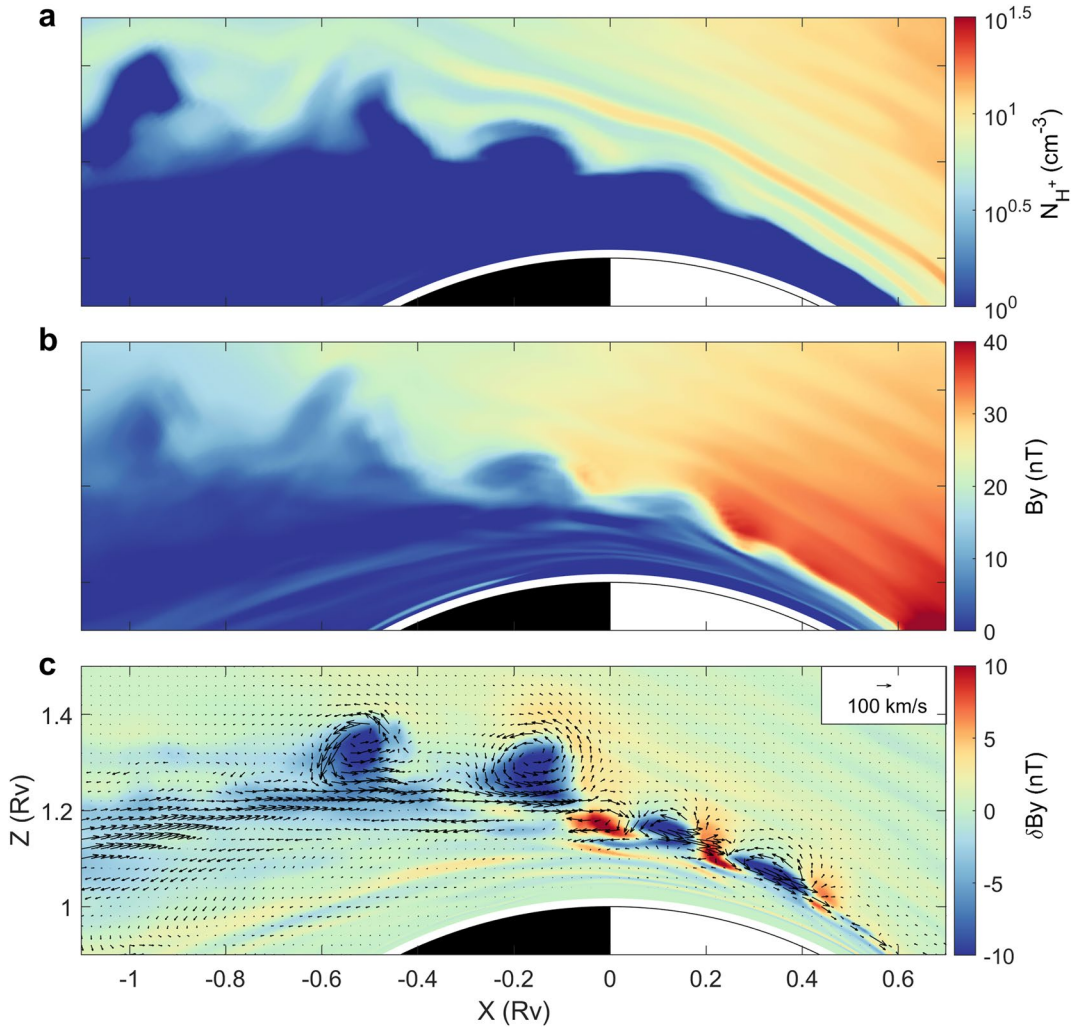

Figure 2. Structure of boundary layer in the X-Z plane at Venus. (a) Distribution of H^+ number density and (b) magnetic field By component in the X-Z plane at 13.8 min simulation time at Venus. (c) The vector field of the H^+ velocity perturbations, $\delta \boldsymbol{V} = \boldsymbol{V} - \langle \boldsymbol{V} \rangle$, is shown with black arrows. The background shows By magnetic field perturbations relative to their average values, $\delta B_y = B_y - \langle B_y \rangle$. $\langle \boldsymbol{V} \rangle$ and $\langle B_y \rangle$ are the 10-min averages at each grid point. See Movie S2 for the related time evolution.

magnetic field (By) (Figure 2b) exhibit similar structures as the distribution of H^+ density. One can also note a very fine trajectory of O^+ in the Movie S3 into the nightside wake with two "lobes" coming from the dayside. The finely structured wake shown in our simulations can help to explore the observed Venusian plasma features such as ionospheric density maxima (Brace et al., 1987) and nightside ionospheric holes (Grebowsky & Curtis, 1981) in the future work.

Figure 2c depicts a snapshot of the By magnetic field perturbations, together with the vectors of the velocity perturbations. At 13.8 min simulation time, four KHI vortexes are present at X = 0.3 Rv, 0.1 Rv, −0.2 Rv, and −0.5 Rv along the boundary layer, respectively. The spatial extension of the vortices increases from dayside to nightside, and becomes most prominent at X = −0.2 Rv. The disappearance of the vortices at the Venusian magnetotail is due to reduced velocity shear at the boundary layer through non-linear evolution of the KHI. An animation of the simulated H^+ density, velocity, magnetic field and pressure is provided in the Movie S2, which shows that the KHI is initiated at dayside and grows convectively along the flank magnetopause with dynamic evolution.

KHI has been proposed to provide important pathway for oxygen ions to escape from a planetary atmosphere without an intrinsic magnetic field. Here we introduced a power spectral method of analysis of the fluctuations

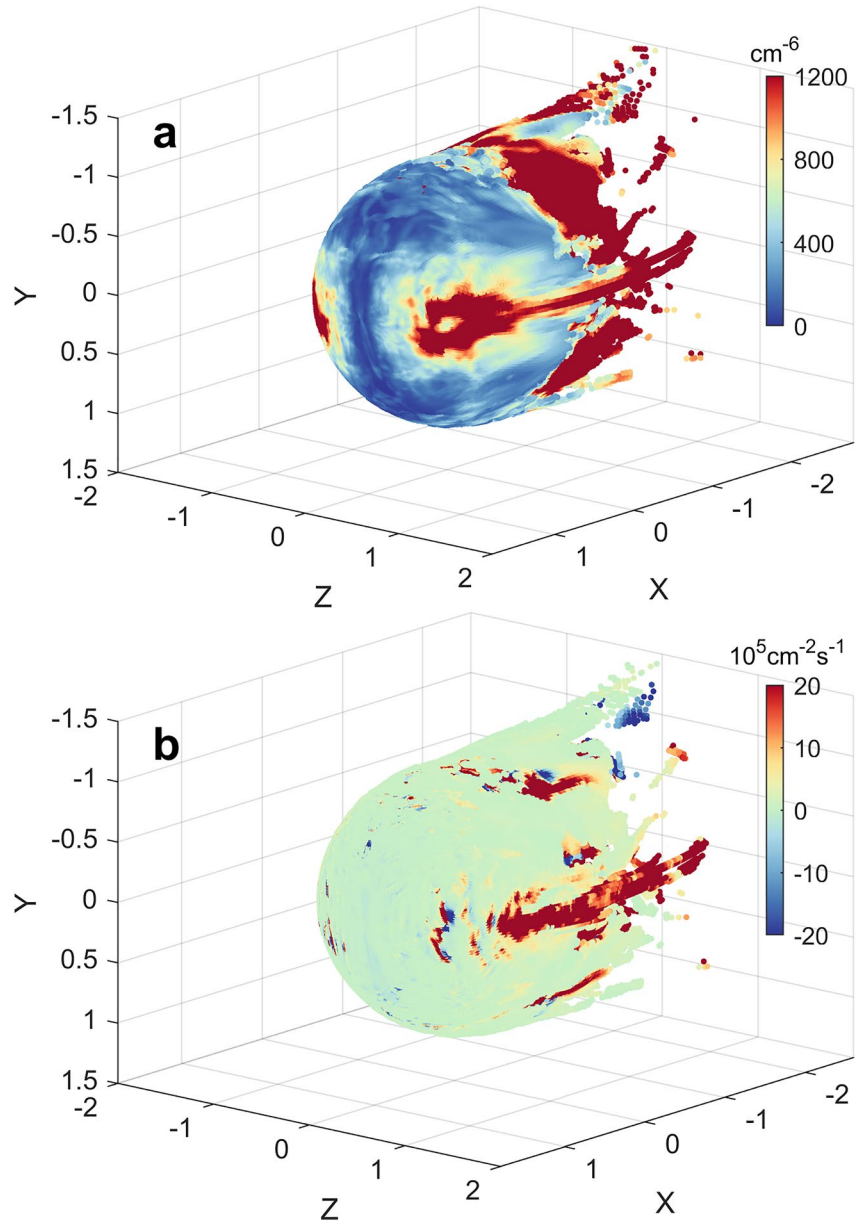

Figure 3. Three-dimensional Venusian ion escape associated with Kelvin-Helmholtz instability. Scatter plot of the three-dimensional distribution of (a) O^+ number density integrated power (IP) and (b) O^+ escaping number flux at the Venusian boundary layer. The three-dimensional boundary layer is determined by the maximum value of IP in each radial direction from Venus center. O^+ escaping number flux is calculated by nV_r where V_r is the radial velocity of O^+ with outward positive.

to represent the properties of the surface waves induced by the KHI, with the integrated power spectral density (PSD) denoting the magnitude of wave activity at the Venusian space environment. Details of the spectral analysis is described in the Method section. Figure 3a displays the KHI activity at the 3D Venusian boundary layer, which is determined by the maximum value of O^+ wave power in each radial direction from the Venus center. Here the O^+ wave power represents the integrated PSD of O^+ mass density. The wave activity is most prominent at the flank region and locates primarily in a narrow band between [−0.3 0.3] Rv in the Y direction, stretching from dayside to the magnetotail. This indicates that the KHI favors more at the low latitude boundary layer (LLBL) if we define the plane perpendicular to IMF (X-Z plane) as the equatorial plane. The wave activity is weak at the subsolar region, due to lower velocity shear between solar wind and ionospheric plasma. At the

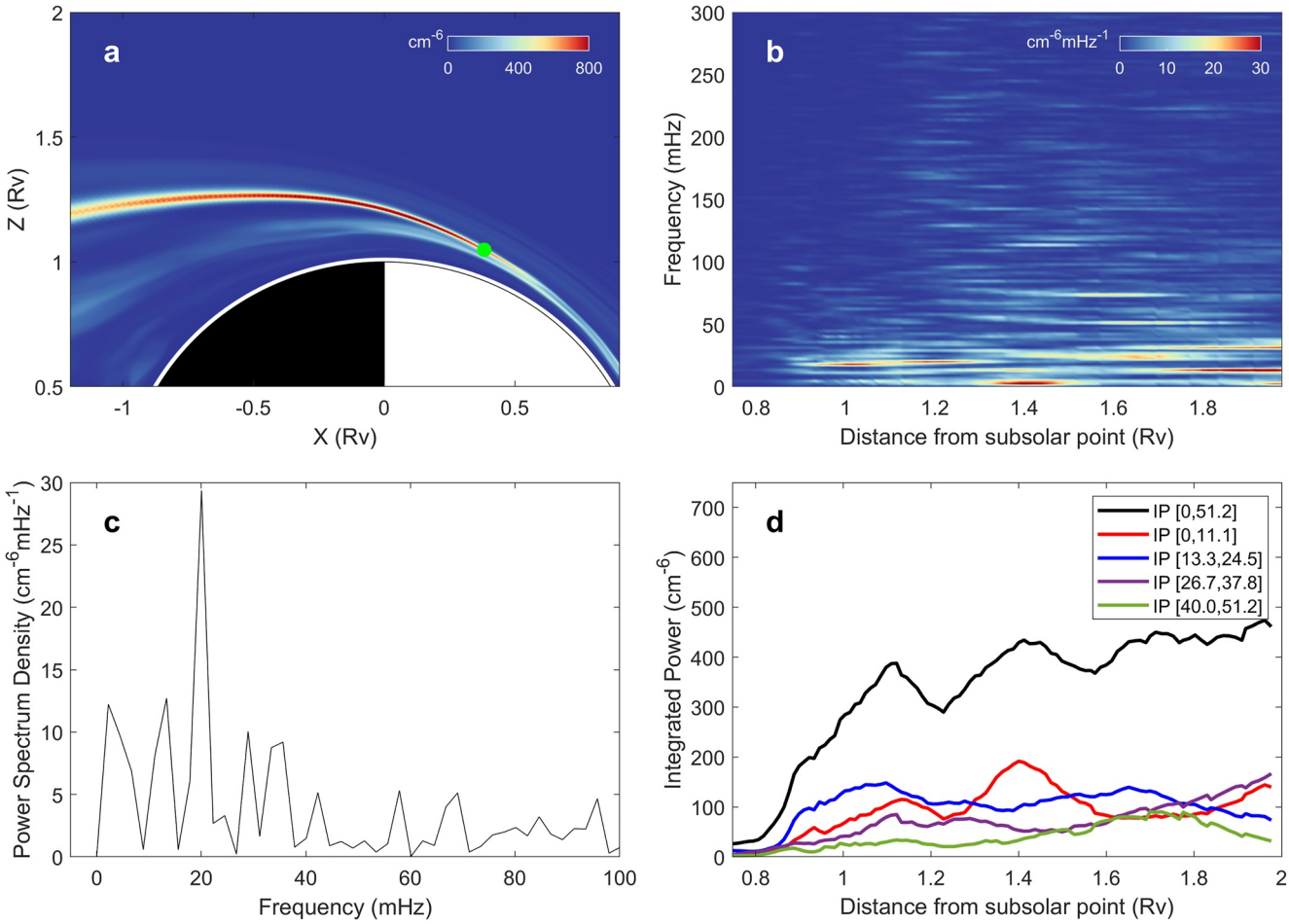

Figure 4. Wave spectrum of Kelvin-Helmholtz instability at Venus. (a), Spatial distribution of integrated power (IP) of the spectrum of H^+ number density in the X-Z plane. The frequency range of the IP is from 0 to 51.2 mHz. (b), Power spectral density distribution as a function of distance from subsolar point and frequency along the boundary layer denoted by the IP maximum in Figure 4a. (c), Power spectrum density variation with frequency at (0.38, 0, 1.05) Rv marked by green dot in Figure 4a. (d), IP fluctuations integrated in different bands from 0 to 51.2 mHz as a function of distance from subsolar point.

magnetotail, large wave power occurs at both low and high latitudes, which is a consequence of the turbulent nature of the Venusian magnetotail.

We explore the three-dimensional global ion escape at Venus in terms of the O^+ ion number flux (nV_r). Figure 3b shows the corresponding O^+ number flux at the boundary layer of Venus. The outflowing O^+ ions are located between [−0.3 0.3] Rv in the Y direction with a narrow stripe, which resembles the distribution of the KHI wave power shown in Figure 3a. However, the O^+ flux is weak at dayside where the wave activity is strongest, since more oxygen ions escape anti-sunward to the nightside. As compared to the LLBL, the simulated outflowing O^+ escaping flux at high latitudes is negligible. For nominal solar wind and interplanetary magnetic field driving conditions, the calculated escaping rate of O^+ at the boundary layer (by integrating number flux within Y ~ [−0.3 0.3] Rv) is 4×10^{24} s^{-1}, which is comparable to the estimated O^+ escape rates in the literature (Luhmann, 1986; Futaana et al., 2017). These results demonstrate the importance of the low latitude ionospheric boundary as the main escape pathway of oxygen ions at the Venusian boundary layer via the KHI.

Figure 4a shows the distribution of the integration of the PSD for the variations in the H^+ number density near the flank in the x-z plane. A distinct narrow layer of the wave perturbations can be seen in the side of the flank from X = 0.4 Rv in the dayside to around X = −1.2 Rv at the magnetotail, representing prominent variations associated with KH instability dominates at the Venusian boundary layer. Moreover, an additional layer appears at the inner part of the aforementioned power maximum layer, with a much weaker integrated power. This is associated with the transport of O^+ from the dayside ionosphere.

A further analysis on the KHI-induced surface waves was given in Figures 4b–4d. We created the analysis by selecting a sequence of PSD density data from X = 0.8 Rv to X = −0.5 Rv along the power maximum line. Figure 4b shows the PSD variations with the distance from the subsolar point and frequency. PSD was mainly distributed between 0 and 51.2 mHz. As the distance goes farther away from the dayside subsolar point, more high frequency waves are generated. The frequency distribution of PSD (Figure 4c) near the terminator, which is marked by the green dot in Figure 4a, peaks at approximately 20 mHz with a PSD of 30 $cm^{-6}Hz^{-1}$, representing a primary period of KHI waves of about 50 s. Other frequency peaks such as 10 mHz, 20 mHz, and 35 mHz are also evident, with weaker PSDs of around 10 $cm^{-6}Hz^{-1}$. Above 40 mHz, the corresponding PSD is relatively small.

The corresponding surface wave power integrated in different frequency bands is given in Figure 4d, as a function of distance from subsolar point along the boundary layer marked by the maximum value of wave power. A two-stage growth of KHI is evident along the magnetopause: a linear growth from 0.82 Rv to 1.17 Rv, followed by a non-linear stage after 1.17 Rv. The overall slope yields a grow rate of 3.69 Rv^{-1} in the linear stage. For the individual modes in different bands, nearly all bands of KHI grows linearly first from the dayside boundary layer to the terminator region at a distance from subsolar point of 1.17 Rv. After that, the KHI develops into non-linear, turbulent structures in the magnetotail. The mode (13.3 mHz 24.5 mHz), which denotes the averaged period of 50 s in Figure 4c, dominant the linear stage while the (0 mHz 11.1 mHz) mode is more prominent when the instability grows non-linearly. This growth feature of KHI is generally similar to that can be seen in the Earth's magnetospheric boundary layer, despite of different spatial scales. Further analysis (not shown here) gives a wave length of 0.8 Rv and a phase speed 0.016 Rv/s (~97 km/s), the latter of which corresponds well with the Earth under a similar solar wind speed (Claudepierre et al., 2008). However, the wave length is much smaller than the Earth's value of 4.2 R_E, possibly due to the much smaller size of the Venusian induced magnetosphere.

4. Discussion and Summary

In this letter, we present the first 3D KHI structures at the Venusian boundary layer, with a newly-developed, global, high-resolution, multi-fluid MHD model for the interaction between the Venusian ionosphere and the upstream solar wind. The KHI is well resolved and exhibits fine evolutions in the 3D global model. The KHI leads to significant escape of oxygen ions through mixing with the solar wind at the low latitude boundary layer of Venus.

Despite Venus is being explored for more than 60 years, the escape of oxygen ions at Venus by solar wind still remains an unclear and fundamental topic. Our results provide a physical explanation for the ion escape and atmospheric loss at Venus. The estimated O^+ escape rate associated with KHI is 4×10^{24} s^{-1}, by comparing the estimated loss rates of O^+ from sputtered model results of O atoms of about 6×10^{24} s^{-1}, the modeled ion pick up escape rates during medium-speed solar wind conditions of about 1.6×10^{25} s^{-1}, as well as the negligible thermal atmospheric escape processes and atmospheric loss by photo-chemically produced oxygen atoms (Lammer et al., 2006; Luhmann & Kozyra, 1991). This indicates that the KHI plays a significant role in removing oxygen ions from Venusian atmosphere. In addition, the downtail outflow resulted from the E × B drift by the solar wind, also contributes to the escape of O^+ from the Venusian ionosphere, as indicated in Movie S3. We have used a Y-Z plane with $X = -1.5$ Rv and estimated the O^+ escape rate of around 2–2.4 $\times 10^{24}$ s^{-1} from this vertical plane. Therefore, together with the KHI-induced escape, the total escape rate is around 6×10^{24} s^{-1}. However, further investigation is required to explore the strong downtail outflux of O^+ in detail in the future work. These results also provide implications for the evolution of other unmagnetized planets, comets, as well as exo-planets.

With improved computing capacity and numerical algorithm, planetary environment models have come to a new era. The recent numerical efforts have revealed important properties of the magnetic field, ion escape and solar wind interactions at Venus (Kallio & Jarvinen, 2012; Kallio et al., 2006; Ma et al., 2013, 2020; Terada et al., 2009). In this work, the sophistication and low numerical dissipation of the new global Venus model allow us to explore the ion escape and boundary layer of the Venusian induced magnetosphere, as well as the physics behind them. Our results exhibit a fine and dynamic evolution of the ions and magnetic fields (see Movies S1–S3) from dayside into the nightside wake via the $\mathbf{E} \times \mathbf{B}$ drift force. Previous estimations of the KHI-induced O^+ escape rate via theoretical estimation (Lammer et al., 2006) and 2-D hybrid models (Terada et al., 2002) provide only a partial view of the loss process with the KHI. The 3D results give insights into how and where the oxygen ions escape from the Venus through the KHI. It is also notable that the oxygen ion escape rate depends on the

conditions of solar activity and solar wind/IMF (Masunaga et al., 2019). The magnetic field and dynamic pressure of the solar wind as well as the source ionospheric O^+ density dominated by the solar EUV irradiation can modulate the KHI behavior and the oxygen ion loss rate, but the general physical process illustrated in this work should not change. Furthermore, with a hybrid model, Terada et al. (2002) illustrated that there was asymmetry in KHI between hemispheres of upward and downward solar wind motional electric fields. This asymmetry is associated with the effect of ion gyro motion, that is, the Hall effect, which is neglected in our multifluid ideal MHD model. This effect is closely related to ion gyroradii (the ratio of ion gyroradius to planetary radius), with estimated H^+ gyroradii of 0.063, 0.1, and 0.43 at Venus, Earth, and Mars, respectively (Ledvina, 2008). Hence, the Hall effect cannot be ignored at Mars (Ma et al., 2019; Najib et al., 2011), but it is reasonable to assume neglecting the Hall effect in the Venus study for large-scale flows (Ledvina, 2008).

The oxygen ion escape with KHI is not easily addressed using observations, especially considering currently there is no existing Venus missions focused on the solar wind interactions. A few observational efforts have been made regarding the KHI at Venus based on Pioneer Venus Orbiter (PVO) and Venus Express (VEX) (Brace et al., 1982; Chong et al., 2018; Pope et al., 2009). The VEX (Svedhem et al., 2007; Titov et al., 2006), has greatly improved our understandings of the Venusian space environment (e.g., Barabash et al., 2007; Zhang et al., 2007, 2012). It was inserted into an elliptical polar orbit around Venus and crossed the induced magnetosphere boundary twice each orbit. However, the observation interval is too limited to examine KH waves. For example, for the spacecraft speed of 10 km/s and an average boundary layer thickness of 1,000 km, the spacecraft can cross the boundary layer in 100 s, which is only one or two periods of the KH waves. Hence, these past satellites could hardly provide a suitable trajectory, measurements, and coverage of the KHI properties as well as the associated oxygen ion escape at Venus. Moreover, the flybys via Venus cannot be understated, since Venus always acts an important body for gravity assist or maneuver for the route to other planets. The BepiColombo for Mercury, Solar Orbiter and Parker Solar Probe for the Sun, and JUICE for Jupiter are equipped with electrostatic analyzers, Langmuir probes and magnetometers and could provide both magnetic field and plasma observations. Also, the flyby satellite has a different trajectory while the VEX is in a polar orbit, providing a potential different opportunity with longer staying in the boundary layer to examine the possible KH evidences.

Acknowledgments
This work was supported by the B-type Strategic Priority Program of the Chinese Academy of Sciences (XDB41000000), the National Natural Science Foundation of China (41831070 and 42188101), the Project of Stable Support for Youth Team in Basic Research Field, CAS (YSBR-018), the pre-research project on Civil Aerospace Technologies No. D020105 funded by China's National Space Administration, and the Open Research Project of Large Research Infrastructures of CAS—"Study on the interaction between low/mid-latitude atmosphere and ionosphere based on the Chinese Meridian Project". T. Dang was supported by the National Natural Science Foundation of China (42174198, 41904138), the National Postdoctoral Program for Innovative Talents (BX20180286), the China Postdoctoral Science Foundation (2018M642525) and the Fundamental Research Funds for the Central Universities. B. Zhang was supported by the General Research Fund (17300719 and 17308520) and the Excellent Young Scientists Fund (Hong Kong and Macau) of the National Natural Science Foundation of China (41922060). The authors are grateful for support from the ISSI/ISSI-BJ workshop "Multi-Scale Magnetosphere–Ionosphere–Thermosphere Interaction". The calculations were completed on the supercomputing system in the Supercomputing Center of University of Science and Technology of China.

Data Availability Statement

The data, plotting code, and materials used in the analyses in this paper are available at website (NSSDC Space Science Article Data Repository: https://dx.doi.org/10.12176/03.99.01701). The model source code is not publicly accessible yet but can be available upon request for the collaboration purpose.

References

Amerstorfer, U. V., Erkaev, N. V., Langmayr, D., & Biernat, H. K. (2007). On Kelvin Helmholtz instability due to the solar wind interaction with unmagnetized planets. *Planetary and Space Science*, *55*(12), 1811–1816. https://doi.org/10.1016/j.pss.2007.01.015

Barabash, S., Fedorov, A., Sauvaud, J. J., Lundin, R., Russell, C. T., Futaana, Y., et al. (2007). The loss of ions from Venus through the plasma wake. *Nature*, *450*, 650–653. https://doi.org/10.1038/nature06434

Brace, L. H., Kasprzak, W. T., Taylor, H. A., Theis, R. F., Russell, C. T., Barnes, A., et al. (1987). The ionotail of Venus: Its configuration and evidence for ion escape. *Journal of Geophysical Research*, *92*(A1), 15–26. https://doi.org/10.1029/JA092iA01p00015

Brace, L. H., Theis, R. F., & Hoegy, W. R. (1982). Plasma clouds above the ionopause of Venus and their implications. *Planetary and Space Science*, *30*(1), 29–37. https://doi.org/10.1016/0032-0633(82)90069-1

Chong, G. S., Pope, S., Walker, S. N., Frahm, R. A., Zhang, T. L., & Futaana, Y. (2018). A statistical study of ionospheric boundary wave formation at Venus. *Journal of Geophysical Research: Space Physics*, *123*, 7668–7685. https://doi.org/10.1029/2018JA025644

Claudepierre, S., Elkington, S., & Wiltberger, M. (2008). Solar wind driving of magnetospheric ulf waves: Pulsations driven by velocity shear at the magnetopause. *Journal of Geophysical Research*, *113*, A05218. https://doi.org/10.1029/2007JA012890

Cloutier, P. A., Tascione, T. F., Daniell, R. E., Jr, Taylor, H. A., & Wolff, R. S. (1983). In *Physics of the interaction of the solar wind with the ionosphere of Venus: Flow/field models* (pp. 941–979). University of Ariz. Press.

Elphic, R. C., & Ershkovich, A. I. (1984). On the stability of the ionopause of Venus. *Journal of Geophysical Research*, *89*, 997–1002. https://doi.org/10.1029/JA089iA02p00997

Fox, J. L., & Sung, K. Y. (2001). Solar activity variations of the Venus thermosphere/ionosphere. *Journal of Geophysical Research*, *106*(A10), 21305–21335. https://doi.org/10.1029/2001ja000069

Futaana, Y., Stenberg Wieser, G., Barabash, S., & Luhmann, J. G. (2017). Solar wind interaction and impact on the Venus atmosphere. *Space Science Reviews*, *212*(3–4), 1453–1509. https://doi.org/10.1007/s11214-017-0362-8

Grebowsky, J. M., & Curtis, S. A. (1981). Venus nightside ionospheric holes: The signatures of parallel electric field acceleration regions? *Geophysical Research Letters*, *8*(12), 1273–1276. https://doi.org/10.1029/GL008i012p01273

Kallio, E., & Jarvinen, R. (2012). Kinetic effects on ion escape at Mars and Venus: Hybrid modeling studies. *Earth Planets and Space*, *64*(2), 157–163. https://doi.org/10.5047/eps.2011.08.014

Kallio, E., Jarvinen, R., & Janhunen, P. (2006). Venus–solar wind interaction: Asymmetries and the escape of O^+ ions. *Planetary and Space Science*, *54*(13–14), 1472–1481. https://doi.org/10.1016/j.pss.2006.04.030

Knudsen, W. C., & Miller, K. L. (1992). The Venus transterminator ion flux at solar maximum. *Journal of Geophysical Research*, *97*, 17165–17167. https://doi.org/10.1029/92JA01460

Lammer, H., Kasting, J. F., Chassefiére, E., Johnson, R. E., Kulikov, Y. N., & Tian, F. (2008). Atmospheric escape and evolution of terrestrial planets and satellites. *Space Science Reviews*, *139*(1–4), 399–436. https://doi.org/10.1007/s11214-008-9413-5

Lammer, H., Lichtenegger, H. I. M., Biernat, H. K., Erkaev, N. V., Arshukova, I. L., Kolb, C., et al. (2006). Loss of hydrogen and oxygen from the upper atmosphere of Venus. *Planetary and Space Science*, *54*, 1445–1456. https://doi.org/10.1016/j.pss.2006.04.022

Ledvina, S. A., Ma, Y.-J., & Kallio, E. (2008). Modeling and simulating flowing plasmas and related phenomena. *Space Science Reviews*, *139*, 143–189. https://doi.org/10.1007/s11214-008-9384-6

Li, Y., & Lu, H. (2019). Evolution of Kelvin-Helmholtz instability on the Venusian ionopause with the influence of Hall effect. *The Astrophysical Journal*, *875*(1), 47. https://doi.org/10.3847/1538-4357/ab10de

Luhmann, J., Fedorov, A., Barabash, S., Carlsson, E., Futaana, Y., Zhang, T. L., et al. (2008). Venus Express observations of atmospheric oxygen escape during the passage of several coronal mass ejections. *Journal of Geophysical Research*, *113*, E00B04. https://doi.org/10.1029/2008JE003092

Luhmann, J., Ledvina, S., Lyon, J., & Russell, C. (2006). Venus O^+ pickup ions: Collected PVO results and expectations for Venus Express. *Planetary and Space Science*, *54*(13), 1457–1471. https://doi.org/10.1016/j.pss.2005.10.009

Luhmann, J. G. (1986). The solar wind interaction with Venus. *Space Science Reviews*, *44*, 241–306. https://doi.org/10.1007/BF00200818

Luhmann, J. G., & Kozyra, J. U. (1991). Dayside pick-up oxygen ion precipitation at Venus and Mars: Spatial distributions, energy deposition and consequences. *Journal of Geophysical Research*, *96*(A4), 5457–5467. https://doi.org/10.1029/90JA01753

Lundin, R. (2011). Ion acceleration and outflow from Mars and Venus: An overview. *Space Science Reviews*, *162*, 309–334. https://doi.org/10.1007/s11214-011-9811-y

Ma, Y., Toth, G., Nagy, A., Luhmann, J., & Russell, C. (2020). Formation and evolution of the large-scale magnetic fields in Venus' ionosphere: Results from a three dimensional global multispecies MHD model. *Geophysical Research Letters*, *47*, e2020GL087593. https://doi.org/10.1029/2020GL087593

Ma, Y. J., Dong, C. F., Toth, G., van der Holst, B., Nagy, A. F., Russell, C. T., et al. (2019). Importance of ambipolar electric field in driving ion loss from Mars: Results from a multifluid MHD model with the electron pressure equation included. *Journal of Geophysical Research: Space Physics*, *124*, 9040–9057. https://doi.org/10.1029/2019JA027091

Ma, Y. J., Nagy, A. F., Russell, C. T., Strangeway, R. J., Wei, H. Y., & Toth, G. (2013). A global multispecies single-fluid MHD study of the plasma interaction around Venus. *Journal of Geophysical Research: Space Physics*, *118*(1), 321–330. https://doi.org/10.1029/2012JA018265

Masunaga, K., Futaana, Y., Persson, M., Barabash, S., Zhang, T. L., Rong, Z. J., & Fedorov, A. (2019). Effects of the solar wind and the solar EUV flux on O^+ escape rates from Venus. *Icarus*, *321*, 379–387. https://doi.org/10.1016/j.icarus.2018.11.017

Masunaga, K., Futaana, Y., Yamauchi, M., Barabash, S., Zhang, T. L., Fedorov, A. O., et al. (2011). O^+ outflow channels around Venus controlled by directions of the interplanetary magnetic field: Observations of high energy O^+ ions around the terminator. *Journal of Geophysical Research*, *116*, A09326. https://doi.org/10.1029/2011JA016705

Merkin, V. G., Lyon, J. G., & Claudepierre, S. G. (2013). Kelvin-Helmholtz instability of the magnetospheric boundary in a three-dimensional global MHD simulation during northward IMF conditions. *Journal of Geophysical Research: Space Physics*, *118*, 5478–5496. https://doi.org/10.1002/jgra.50520

Michael, A. T., Sorathia, K. A., Merkin, V. G., Nykyri, K., Burkholder, B., Ma, X., et al. (2021). Modeling Kelvin-Helmholtz instability at the high-latitude boundary layer in a global magnetosphere simulation. *Geophysical Research Letters*, *48*, e2021GL094002. https://doi.org/10.1029/2021GL094002

Möstl, U. V., Erkaev, N. V., Zellinger, M., Lammer, H., Gröller, H., Biernat, H. K., & Korovinskiy, D. (2011). The Kelvin–Helmholtz instability at Venus: What is the unstable boundary? *Icarus*, *216*(2), 476–484. https://doi.org/10.1016/j.icarus.2011.09.012

Najib, D., Nagy, A. F., Tóth, G., & Ma, Y. (2011). Three-dimensional, multifluid, high spatial resolution MHD model studies of the solar wind interaction with Mars. *Journal of Geophysical Research*, *116*, A05204. https://doi.org/10.1029/2010JA016272

Nordström, T., Stenberg, G., Nilsson, H., Barabash, S., & Zhang, T. L. (2013). Venus ion outflow estimates at solar minimum: Influence of reference frames and disturbed solar wind conditions. *Journal of Geophysical Research: Space Physics*, *118*, 3592–3601. https://doi.org/10.1002/jgra.50305

Pope, S. A., Balikhin, M. A., Zhang, T. L., Fedorov, A. O., Gedalin, M., & Barabash, S. (2009). Giant vortices lead to ion escape from Venus and re-distribution of plasma in the ionosphere. *Geophysical Research Letters*, *36*(7), L07202. https://doi.org/10.1029/2008GL036977

Shizgal, B. D., & Arkos, G. G. (1996). Nonthermal escape of the atmospheres of Venus, Earth, and Mars. *Review of Geophysics*, *34*(4), 483–505. https://doi.org/10.1029/96RG02213

Sorathia, K. A., Merkin, V. G., Panov, E. V., Zhang, B., Lyon, J. G., Garretson, J., et al. (2020). Ballooning-interchange instability in the near-Earth plasma sheet and auroral beads: Global magnetospheric modeling at the limit of the MHD approximation. *Geophysical Research Letters*, *47*, e2020GL088227. https://doi.org/10.1029/2020GL088227

Svedhem, H., Titov, D. V., McCoy, D., Lebreton, J.-P., Barabash, S., Bertaux, J.-L., et al. (2007). The first European mission to Venus. *Planetary and Space Science*, *55*, 1636–1652. https://doi.org/10.1016/j.pss.2007.01.013

Terada, N., Machida, S., & Shinagawa, H. (2002). Global hybrid simulation of the Kelvin-Helmholtz instability at the Venus ionopause. *Journal of Geophysical Research*, *107*(A12), 1471. https://doi.org/10.1029/2001JA009224

Terada, N., Shinagawa, H., Tanaka, T., Murawski, K., & Terada, K. (2009). A three-dimensional, multispecies, comprehensive MHD model of the solar wind interaction with the planet Venus. *Journal of Geophysical Research*, *114*, A09208. https://doi.org/10.1029/2008JA013937

Thomas, V. A., & Winske, D. (1991). Kinetic simulation of the Kelvin-Helmholtz instability at the Venus ionopause. *Geophysical Research Letters*, *18*, 1943–1946. https://doi.org/10.1029/91GL02552

Titov, D. V., Svedhem, H., Koschny, D., Hoofs, R., Barabash, S., Bertaux, J.-L., et al. (2006). Venus Express science planning. *Planetary and Space Science*, *54*, 1279–1297. https://doi.org/10.1016/j.pss.2006.04.017

Walker, S. N., Balikhin, M. A., Zhang, T. L., Gedalin, M. E., Pope, S. A., Dimmock, A. P., & Fedorov, A. O. (2011). Unusual nonlinear waves in the Venusian magnetosheath. *Journal of Geophysical Research*, *116*(A1), A01215. https://doi.org/10.1029/2010JA015916

Way, M. J., Del Genio, A. D., Kiang, N. Y., Sohl, L. E., Grinspoon, D. H., Aleinov, I., et al. (2016). Was Venus the first habitable world of our solar system? *Geophysical Research Letters*, *43*, 8376–8383. https://doi.org/10.1002/2016GL069790

Wolff, R. S., Goldstein, B. E., & Yeates, C. M. (1980). The onset and development of Kelvin—Helmholtz instability at the Venus ionopause. *Journal of Geophysical Research*, *85*, 7697–7707. https://doi.org/10.1029/JA085iA13p07697

Zhang, B., Sorathia, K. A., Lyon, J. G., Merkin, V. G., Garretson, J. S., & Wiltberger, M. (2019). Gamera: A three-dimensional finite-volume MHD solver for non-orthogonal curvilinear geometries. *The Astrophysical Journal—Supplement Series*, *244*(1), 20. https://doi.org/10.3847/1538-4365/ab3a4c

Zhang, T., Lu, Q., Baumjohann, W., Russell, C., Fedorov, A., Barabash, S., et al. (2012). Magnetic reconnection in the near Venusian magnetotail. *Science*, *336*(6081), 567–570. https://doi.org/10.1126/science.1217013

Zhang, T. L., Delva, M., Baumjohann, W., Auster, H.-U., Carr, C., Russell, C. T., et al. (2007). Little or no solar wind enters Venus' atmosphere at solar minimum. *Nature*, *450*(7170), 654–656. https://doi.org/10.1038/nature06026

References From the Supporting Information

Alge, E., Adams, N. G., & Smith, D. (1983). Measurements of the dissociative recombination coefficients of O_2+, NO^+ and NH_4^+ in the temperature range 200–600K. *Journal of Physics B: Atomic and Molecular Physics*, *16*(8), 1433–1444. https://doi.org/10.1088/0022-3700/16/8/017

Anicich, V. G. (1993). Evaluated bimolecular ion-molecule gas phase kinetics of positive ions for use in modeling planetary atmospheres, cometary comae, and interstellar clouds. *Journal of Physical and Chemical Reference Data*, *22*(6), 1469–1569. https://doi.org/10.1063/1.555940

Brambles, O. J., Lotko, W., Damiano, P. A., Zhang, B., Wiltberger, M., & Lyon, J. (2010). Effects of causally driven cusp O^+ outflow on the storm time magnetosphere-ionosphere system using a multifluid global simulation. *Journal of Geophysical Research*, *115*, A00J04. https://doi.org/10.1029/2010JA015469

Fehsenfeld, F. C., Dunkin, D. B., & Ferguson, E. E. (1970). Rate constants for the reaction of CO2$^+$ with O, O_2 and NO; N_2^+ with O and NO; and O_2^+ with NO. *Planetary and Space Science*, *18*(8), 1267–1269. https://doi.org/10.1016/0032-0633(70)90216-3

Fox, J. L., & Sung, K. Y. (2001). Solar activity variations of the Venus thermosphere/ionosphere. *Journal of Geophysical Research*, *106*(A10), 21305–21335. https://doi.org/10.1029/2001ja000069

Kulsrud, R. M. (1983). *MHD description of plasma handbook of plasma physics*. North Holland Publishing. https://doi.org/10.2172/7072860

Ma, Y. J., Nagy, A. F., Russell, C. T., Strangeway, R. J., Wei, H. Y., & Toth, G. (2013). A global multispecies single-fluid MHD study of the plasma interaction around Venus. *Journal of Geophysical Research*, *118*(1), 321–330. https://doi.org/10.1029/2012JA018265

Mehr, F. J., & Biondi, M. A. (1969). Electron temperature dependence of recombination of O_2^+ and N_2^+ ions with electrons. *Physical Review*, *181*(1), 264–271. https://doi.org/10.1103/PhysRev.181.264

Richards, P. G., Fennelly, J. A., & Torr, D. G. (1994). EUVAC: A solar EUV flux model for aeronomic calculations. *Journal of Geophysical Research*, *99*(A5), 8981–8992. https://doi.org/10.1029/94JA00518

Schunk, R. W., & Nagy, A. F. (2000). *Ionospheres: Physics, plasma physics and chemistry*. Cambridge University Press. https://doi.org/10.1017/cbo9780511551772

Viggiano, A. A., Ehlerding, A., Hellberg, F., Thomas, R. D., Zhaunerchyk, V., Geppert, W. D., et al. (2005). Rate constants and branching ratios for the dissociative recombination of CO_2^+. *The Journal of Chemical Physics*, *122*(22), 226101. https://doi.org/10.1063/1.1926283

Viggiano, A. A., Morris, R. A., Doren, M. V., & Paulson, J. F. (1992). Temperature, kinetic energy, and internal energy dependences of the rate constant and branching fraction for the reaction of O^+ (4S) with CO_2. *The Journal of Chemical Physics*, *96*(1), 270–274. https://doi.org/10.1063/1.462514